BNL-112140-2016-JA

Towards Uniformly Dispersed Battery Electrode Composite Materials: Characteristics and Performance

Yo Han Kwon[1], Matthew M. Huie[5], Dalsu Choi[1], Mincheol Chang[1], Amy C. Marschilok[4,5], Kenneth J. Takeuchi[4,5], Esther S. Takeuchi[4,5,6] and Elsa Reichmanis[1,2,3]

[1]Department of Chemical and Biomolecular Engineering, Georgia Institute of Technology, Atlanta, GA USA
[2]Department of Chemical and Biochemistry, Georgia Institute of Technology, Atlanta, GA USA
[3]Department of Materials Science and Engineering, Georgia Institute of Technology, Atlanta, GA USA
[4]Department of Chemistry, Stony Brook University, Stony Brook, NY USA
[5]Department of Materials Science and Engineering, Stony Brook University, Stony Brook, NY USA
[6]Energy Sciences Directorate, Brookhaven National Laboratory, Upton, NY USA

Submitted to ACS Applied Materials & Interfaces

January 2016

Energy and Photon Sciences Directorate

Brookhaven National Laboratory

U.S. Department of Energy
Office of Science, Basic Energy Sciences

DISCLAIMER

This report was prepared as an account of work sponsored by an agency of the United States Government. Neither the United States Government nor any agency thereof, nor any of their employees, nor any of their contractors, subcontractors, or their employees, makes any warranty, express or implied, or assumes any legal liability or responsibility for the accuracy, completeness, or any third party's use or the results of such use of any information, apparatus, product, or process disclosed, or represents that its use would not infringe privately owned rights. Reference herein to any specific commercial product, process, or service by trade name, trademark, manufacturer, or otherwise, does not necessarily constitute or imply its endorsement, recommendation, or favoring by the United States Government or any agency thereof or its contractors or subcontractors. The views and opinions of authors expressed herein do not necessarily state or reflect those of the United States Government or any agency thereof.

Towards Uniformly Dispersed Battery Electrode Composite Materials: Characteristics and Performance

Yo Han Kwon,[†] Matthew M. Huie,[§] Dalsu Choi,[†] Mincheol Chang,[†] Amy C. Marschilok,[‡,§] Kenneth J. Takeuchi,[‡,§] Esther S. Takeuchi,*[,‡,§,‖] and Elsa Reichmanis*[,†,††,†††]

[†]Department of Chemical and Biomolecular Engineering, Georgia Institute of Technology, Atlanta, GA 30332, USA

[††]Department of Chemical and Biochemistry, Georgia Institute of Technology, Atlanta, GA 30332, USA

[†††]Department of Materials Science and Engineering, Georgia Institute of Technology, Atlanta, GA 30332, USA

[‡]Department of Chemistry, Stony Brook University, Stony Brook, NY 11794, USA

[§]Department of Materials Science and Engineering, Stony Brook University, Stony Brook, NY 11794, USA

[‖]Energy Sciences Directorate, Brookhaven National Laboratory, Upton, NY 11973

ABSTRACT

Battery electrodes are complex mesoscale systems, comprised of electroactive components, conductive additives, and binders. In this report, methods for processing electrodes with dispersion of the components are described. To investigate the degree of material dispersion, a spin coating technique was adopted to provide a thin, uniform layer which enabled observation of the morphology. Distinct differences in the distribution profile of the electrode components arising from individual materials physical affinities were readily identified. Hansen solubility parameter (HSP) analysis revealed pertinent surface interactions associated with materials dispersivity. Further studies demonstrated that HSPs can provide an effective strategy to identify surface modification approaches for improved dispersions of battery electrode materials. Specifically, introduction of surfactant-like functionality such as oleic acid (OA) capping and P3HT conjugated polymer wrapping, on the surface of nanomaterials significantly enhanced material dispersity over the composite electrode. The approach to the surface treatment on the basis of HSP study can facilitate design of composite electrodes with uniformly dispersed morphology, and may contribute to enhancing their electrical and electrochemical behaviors. The conductivity of the composites and their electrochemical performance was also characterized. The study illustrates the importance of considering electronic conductivity, electron transfer as well as ion transport in the design of environments incorporating active nanomaterials.

KEYWORDS: nanomaterials, capping agent, poly(3-hexylthiophene), dispersion, morphology processing, Hansen solubility parameters, Lithium-ion battery

INTRODUCTION

Identification of effective strategies to reduce electrode resistance and elevate the energy capacity of Li-ion batteries, which are commonly used in mobile devices and electric vehicles (EVs), is of significant interest.[1,2] Nanomaterials are considered to be one promising approach to achieve these goals. Specifically, the use of nanomaterials offers the advantages associated with a short Li^+ diffusion path that can facilitate the charge transfer process and enhance the utilization of active sites even at high power rates. [3–7]

Despite demonstration of desirable characteristics, the anticipated benefits associated with the use of nanometer-scale materials have yet to be fully realized, and in some cases, composite battery electrode performance has been shown to be inferior for nanomaterials vs. their bulk couterparts.[8] Aggregation and materials dispersion have been suggested as leading factors that impact the performance of composite electrode materials. For instance, it has been shown that more uniformly dispersed materials exhibit improved performance attributes.[8–10] Specifically, nano-sized conductive additives tend to readily agglomerate during battery electrode processing, thereby hindering homogeneous current distribution over the electrode and negatively influencing electrochemistry.[5,11] In fact, mesoscale modeling has shown that both the size of the parent particle (crystallite) and the size of the aggregate must be considered to accurately describe battery performance.[12] Closer inspection of electrode structure offers additional insight. Battery electrodes are generally composite materials, wherein the active materials are mixed with conductive additives to create an interconnected, percolated conductive network. An inactive polymeric binder provides for structural integrity.[5,7] The interconnected conductive pathways are expected to be related to particle dispersion within the polymeric medium which may in turn impact electrochemical performance.

To realize the full potential afforded by nanomaterials, it is necessary to fabricate and

characterize composite electrodes with varying degrees of dispersion at the nano- through mesoscales. Here, two approaches are used to gain important perspectives on the impact of dispersity and morphology on composite electrode performance. Investigations focus on i) how to enhance materials dispersity in the battery electrode and ii) how morphological differences link to their electrical properties and performance.

The high surface area and attractive forces (van der Waals) associated with nanomaterials are known to impede their dispersion and from a thermodynamic perspective, facilitate agglomeration. Thus, simple physical techniques such as ultra-sonication may be insufficient to achieve stable, homogeneous nanomaterial dispersions and chemical routes may be required.[23] To date, efforts to enhance dispersivity of battery electrode materials have been limited; however, extensive efforts associated with the uniform dispersion of nanomaterials used in photovoltaic devices[15,16] and potential biomedical applications[18,19] have been reported. It has been found that the propensity of nanoparticles such as Au, CdSe, SiO, ZnO, TiO_2, and Fe_3O_4 to agglomerate can be reduced by coating them with suitable capping agents.[13–22] Carbon nanomaterials, including carbon nanotubes (CNTs) and carbon nanofibers (CNFs), can be dispersed effectively by judicious choice of solvent, use of surfactants, surface functionalization, and/or wrapping with conjugated polymers such as poly(9,9-dialkylfluorene) (PF) or regioregular poly(3-alkylthiophene) (P3AT). In the latter case, interactions between the π-conjugated chains and carbon surface, and the presence of alkyl side chains both assist effective dispersion.[23–26]

Thus, to inhibit the agglomeration process and achieve stable nanomaterials dispersions, surfactant-like moieties can be introduced onto their surface with physical or chemical means. This same fundamental principle may also provide for improved materials dispersion in the case of battery electrode composite materials. To evaluate the impact of nanomaterials dispersion in electrode applications, Fe_3O_4 nanoparticles (8nm) capped with oleic acid (OA-Fe_3O_4) and poly(3-

hexylthiophene) (P3HT) were chosen as the active material and conjugated polymer, respectively. Oleic acid (OA) and P3HT provide for surfactant-like functionality for Fe_3O_4 and carbon additives. Hansen Solubility Parameter (HSP) analysis suggests that OA-Fe_3O_4 and carbon/P3HT will be well-mixed in the final electrode.

To investigate electrode materials morphology, a spin-coating technique was used to prepare the composite thin-films. Typical coating methods such as blade coating, dip coating, and drop casting form dense, thick film layers that are inappropriate to adequately visualize distinctive morphologies and differentiate the degree of material dispersity in the electrode. The spin coating method affords a thin, uniform film layer, and morphological differences can be easily detected even by optical microscopy (OM) at low magnification. While battery electrode performance cannot be directly measured using the spin-coating technique, the method is a facile approach to visualize more distinct images of the electrode components in order to judge materials distribution, and help interpret the impact of materials size and distribution on electrical and electrochemical behavior in a dense electrode.

Poly(3-hexylthiophene) (P3HT) is an interesting conductive polymer for a battery cathode material because polythiophenes have relatively small band gaps and high conductivities.[27] Additionally, P3HT has a low reduction potential (0.5 V vs. Li/Li^+)[28] which suggests that this conductive polymer should remain conductive at operating voltages above 0.5 V. Block copolymers of P3HT and poly(ethylene oxide) (P3HT-b-PEO) have been investigated for Li-ion batteries. P3HT-b-PEO block copolymers phase separate to form a lamellar phase which combines the high intrinsic electronic conductivity of P3HT with regions of PEO which are conducive for Li^+ ion diffusion.[29] P3HT-b-PEO has been used as a binder with several cathode materials.[30–32] The block copolymer displayed high electronic and ionic conductivities[29,33,34] as well as mechanical stability.[32] However, electronic conductivity of the $LiFePO_4$/P3HT-b-PEO cathode dropped from 10^{-4} S/cm to

10^{-7} S/cm when the operating voltage dropped below 3.3 V during discharge.[30] P3HT has also been copolymerized with sulfur for use as an additive (not as a binder) in Li-S batteries.[35] The addition of sulfur-P3HT copolymer to the electrode improved battery cycle life and high rate performance which was attributed to the inhibited dissolution of polysulfides.

The dispersing agent used here was oleic acid ($C_{18}H_{34}O_2$), a long organic chain with a carboxylic acid functional group which has been used as a surfactant to promote nanoparticle formation and reduced nanoparticle agglomeration. Reducing agglomeration is important for electrode performance as it shortens diffusion pathways for ions to reach the crystalline active material. There are some studies of oleic acid-coated active materials, but the electrochemical impact of the coating is still unclear. Oleic acid coated Fe_2O_3 in a Li-ion battery displayed better capacity and high rate performance compared to uncoated Fe_2O_3.[36] This result was attributed to the capacitive nature of oleic acid which formed a surface double layer inducing a pseudo-capacitance interfacial charging event. Guo et al. used oleic acid to coat Mn_3O_4 for a capacitor and found the oleic acid helped form uniform microspheres with a capacitance improvement.[37] The interaction of oleic acid with conductive polymers is not broadly researched, but one study of oleic acid-stabilized silver nanoparticles with polythiophenes in organic thin-film transistors,[38] found that the presence of oleic acid with polythiophene improved electrical conductivity.

Through investigating the role of an oleic acid capping agent introduced on the magnetite surface in the performance with both conductive and nonconductive polymer binders, the approach presented here aims to provide fundamental insights into the mechanistic foundation for efforts associated with uniform dispersion in battery electrode applications, especially for the efficient incorporation with electroactive nanomaterials components.

RESULTS AND DISCUSSION

Materials Morphology. In general, the dense morphology of battery electrodes inhibits the ability to differentiate the degree of materials dispersion within the composite. Using a spin coating technique, well-known but unfamiliar in the battery field, battery electrode materials dispersion was analyzed and evaluated. While indirect, the method enables deposition of a thin, uniform layer of electrode material, which facilitates characterization of the distribution of the individual electrode components. Poly(vinylidene difluoride) (PVDF) and P3HT were used as the binder materials. PVDF is widely used as the binder in Li-ion battery electrodes due to its good electrochemical stability and high binding adhesion to the electrode materials and current collectors.[39] Thus, the PVDF system was used as standard reference; N-methyl-2-pyrrolidone (NMP) was the solvent. P3HT is a potentially attractive conducting polymer binder alternative.

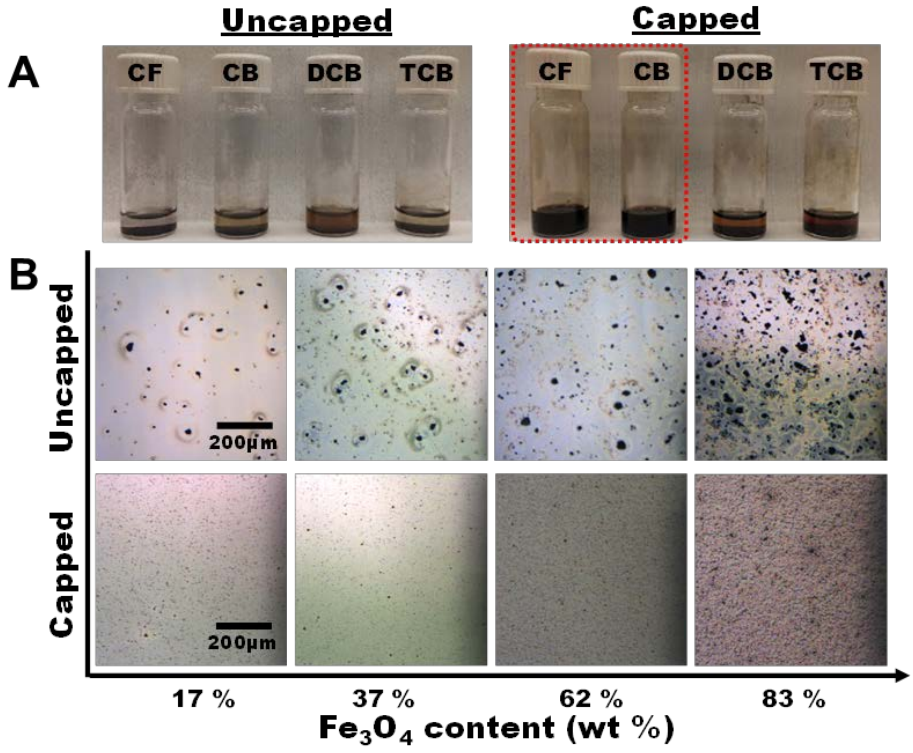

Figure 1. (A) Dispersion state in different solvents. Capped Fe_3O_4 is well-dispersed in chloroform and chlorobenzene. (B) OM images of uncapped Fe_3O_4/P3HT composites and OA-capped Fe_3O_4/P3HT composites. Samples were prepared by spin coating on glass substrates using chloroform solvent.

To minimize agglomeration effects and promote the uniform distribution of active material, Fe_3O_4 nanoparticles were capped with oleic acid. Oleic acid was selected because previous studies showed that the OA –COOH moieties readily bind to surface -OH functionalities present on many inorganic materials thereby improving their dispersion characteristics.[21,22] The dispersion state of OA-capped and uncapped Fe_3O_4 nanoparticles was evaluated in a range of solvents known to dissolve the conjugated polymer, P3HT; namely, chloroform (CF), chlorobenzene (CB), dichlorobenzene (DCB), and trichlorobenzene (TCB). As shown in **Figure 1A**, the uncapped nanoparticles failed to disperse and simply precipitated, whereas the OA-capped nanoparticles were well-dispersed in CF and CB. Subsequent studies related to the conjugated polymer-based electrode system focused on chloroform because it solubilizes P3HT more effectively.

To visualize the dispersion state of the capped vs. uncapped Fe_3O_4, Fe_3O_4/P3HT composite films were coated onto glass substrates by spin-coating (1500 rpm, 60 sec) and the resultant thin-film morphologies were observed by optical microscopy. Aggregates were observed in all films prepared with uncapped Fe_3O_4 and aggregate size increased with increased Fe_3O_4 content. For the proportions investigated here, aggregate size ranged from approximately 2 to 40 µm. Aggregation was not observed for the oleic acid capped materials: OA-Fe_3O_4 appears uniformly distributed regardless of the proportion of active material. Both OA-Fe_3O_4 and P3HT are expected to be hydrophobic and may have similar physical affinities, which may in turn facilitate uniform dispersion.

Figure 2 presents the observed thin-film morphologies for P3HT- *vs.* PVDF-based composites formulated with the respective polymers, carbon and magnetite where the carbon content of each film was changed. The absolute amount/weight of OA-Fe_3O_4 and Super-P carbon additives were fixed. The volume percent of carbon was determined from the weight percent using the material density (Fe_3O_4: 5.0 g/cc, Super-P carbon additive: 1.85 g/cc, P3HT: 1.10 g/cc, PVDF: 1.78 g/cc). The

composite thin-films were prepared by spin-coating (1500 rpm, 60 sec) from chloroform and NMP for the P3HT and PVDF systems, respectively. Coating parameters (i.e. spin speed, colloidal concentration) are known to affect the density and morphology of resultant films; higher spin speeds and lower colloidal concentrations generally afford thinner films that are spread out and have more sparsely dispersed nanoparticles.[40,41] From this perspective, the processing parameters (spin coating: 1500 rpm for 60 sec, solid content: 3.4 wt%) adopted here to explore thin film morphology are expected to provide for the appropriate degree of materials dispersion to be discernible. Furthermore, while substrate and solvent properties (i.e. vapor pressure, boiling point, and evaporation rate) may also affect the evolution of thin-film morphology, the effects will be minimized due to centrifugal forces associated with the spinning process; the deposited material spreads rapidly and solvent quickly evaporates, thereby suppressing solvent evaporation effects and adequately enabling visualization of the physical affinities among component materials.

Figures 2A and 2B present optical microscopic images of OA-Fe_3O_4/carbon/polymer and carbon/polymer composite thin-films, respectively. Distinct morphological differences can be discerned between the P3HT and PVDF-based systems. In PVDF, OA-Fe_3O_4 nanoparticles appear as brown-colored aggregates and the carbon additive appears black. When the carbon content is increased incrementally, carbon aggregate size also increases and appears to cover the region occupied by OA-Fe_3O_4. Further, the desired conductive network appears to be disconnected due to nanoparticle agglomeration. The resulting morphology might be expected to interfere with effective current distribution throughout a PVDF-based composite electrode. In contrast, the P3HT-based system presents a uniformly dispersed morphology irrespective of carbon content. By augmenting the proportion of carbon additive, an apparently percolated, interconnected conductive network was produced. The percolation network formed by the spherical carbon additives (~50nm, 49 vol. %) was readily visualized by atomic force microscopy (AFM) (**Figure 2C**). Moreover, AFM observation (**Figure S1**) provides for the well-connected, electronic carbon additive networks, together with OA-

Fe_3O_4 nanoparticles. The results strongly suggest that the OA-surface treatment of Fe_3O_4 nanoparticles might also influence the interactions between OA-Fe_3O_4 and the conductive network due to their similar physical affinities.

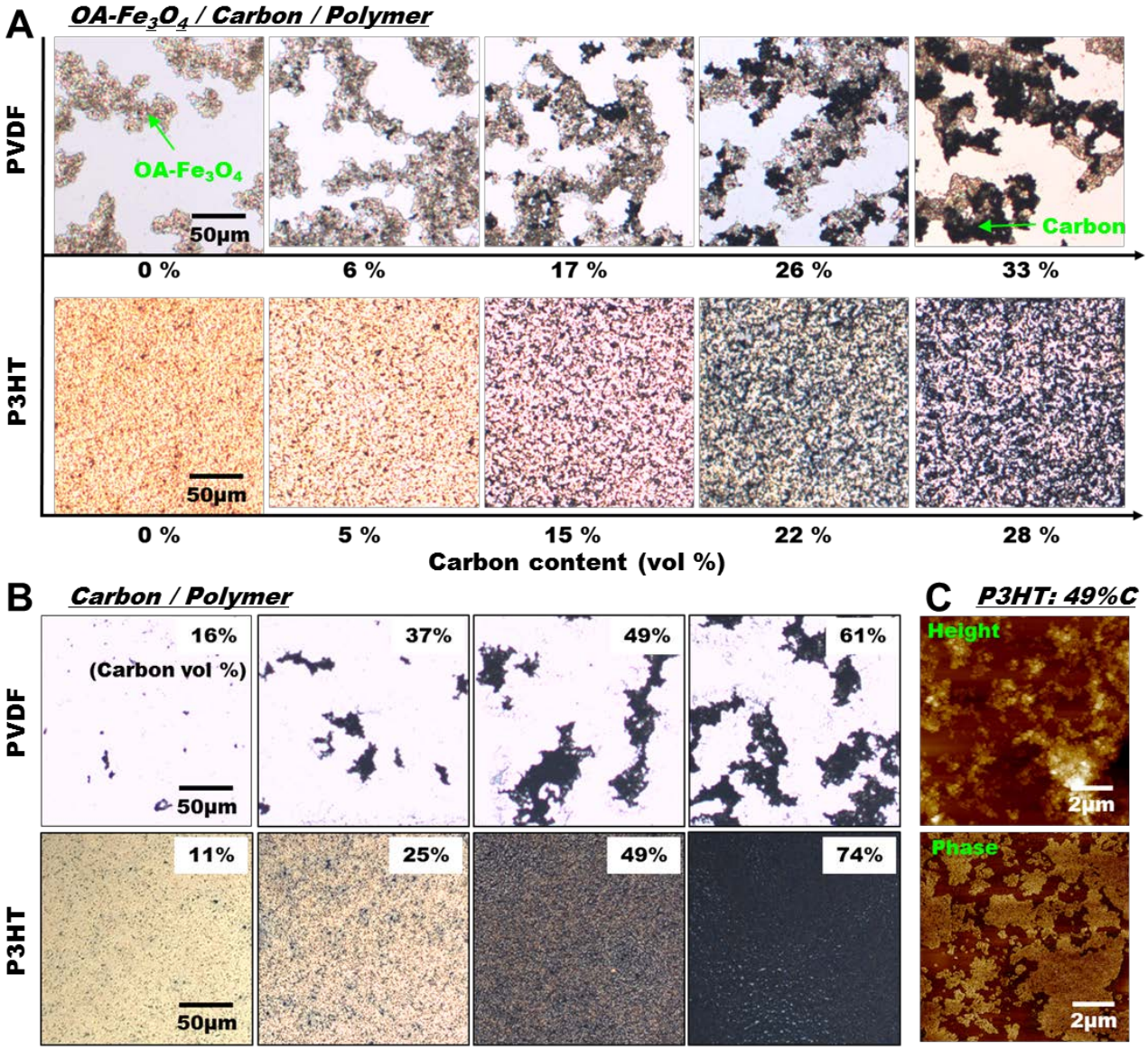

Figure 2. (A) OM images of OA-Fe_3O_4/carbon/polymer composites according to different carbon content. The absolute amount of OA-Fe_3O_4 and polymer was kept constant. The volume percent of carbon content was converted by material density. (B) OM images of carbon/polymer composites with different carbon content. P3HT system shows much more favorable uniform dispersion than PVDF system. (C) Tapping mode AFM height and phase images of 49 vol. % of carbon/P3HT composite film, demonstrating the conductive percolation networks.

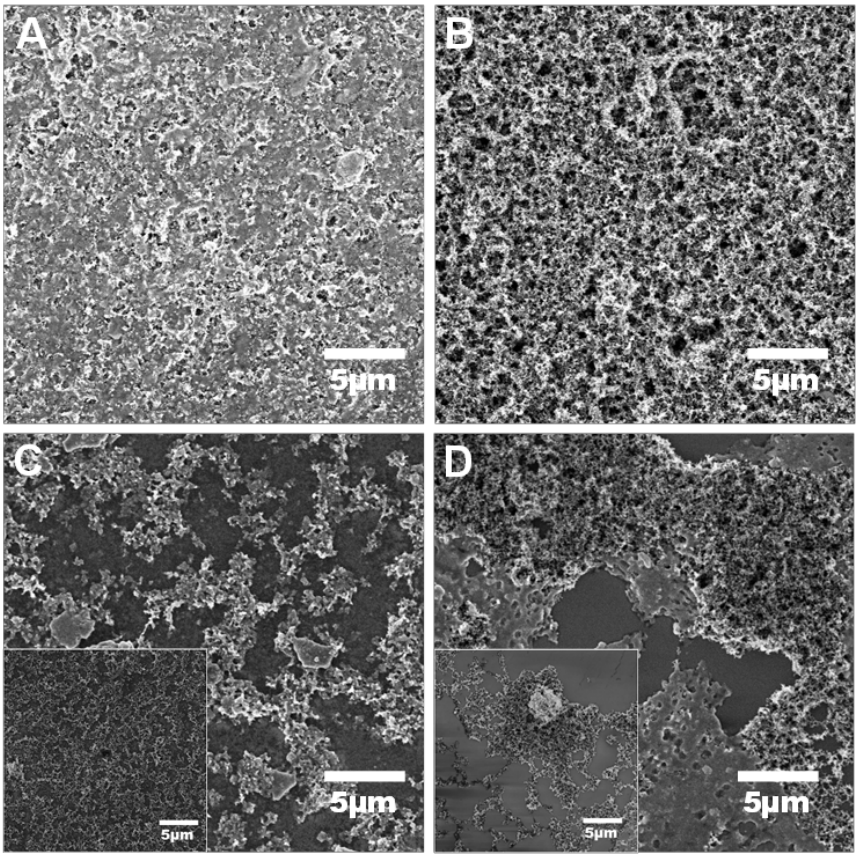

Figure 3. FE-SEM images of OA-Fe_3O_4/carbon/polymer composite electrodes (Top view). (A) P3HT-based electrode (blade coating). (B) PVDF-based electrode (blade coating). (C) P3HT-based electrode (spin coating, inset: carbon/P3HT). (D) PVDF-based electrode (spin coating, inset: carbon/PVDF). The spin coated material shows the distinct morphology associated with the material dispersion state.

Figure 3 shows Field Emission-Scanning Electron Microscopy (FE-SEM) images of OA-Fe_3O_4/carbon/P3HT and OA-Fe_3O_4/carbon/PVDF battery composite electrodes fabricated by doctor blade (**Figure 3A and 3B**) and spin coat (**Figure 3C and 3D**) processes, respectively. Morphological differences between the two systems are difficult to observe from the doctor blade samples (**Figure 3A, B)** due to their thick, dense nature. Alternatively, distinct morphological differences are apparent with the thinner, spin-coated alternatives (**Figure 3C, D**): the components appear better dispersed within P3HT vs. PVDF, which supports the optical imaging results (**Figure 2**).

As shown in **Figure 2B** and the inset image of **Figure 3C**, the spherical, nanosized carbon

additives appear relatively well-dispersed within P3HT. Presumably, the π-conjugated regioregular P3HT backbone interacts with carbon π-electrons residing at the surface, while the solubilizing alkyl side chains help to maintain their dispersion state.[24] The dispersion of OA-Fe_3O_4 nanoparticles in P3HT is likely influenced by similar physical affinities between the hydrophobic tail of the capping agent and the P3HT side chains. The morphology results suggest that in order to achieve uniform and stable battery electrode nanomaterials dispersions, consideration should be given to materials surface physical affinities/interactions. In addition, introduction of a surfactant-like species on the respective nanomaterial surfaces, whether through use of a capping agent or wrapping by a polymer chain, to manipulate that physical affinity in an advantageous manner is especially important.

Physical Affinity Relationship. Physical compatibility between materials that comprise a battery electrode is expected to greatly influence the materials interfacial properties, as will the degree of material dispersion. One approach to examine the physical affinity between different materials uses Hansen solubility parameter (HSP) analysis. Typically, materials with similar HSP values exhibit high physical affinities or rather, compatibility.[42] The extent of the similarity can serve as a measure of the extent of interaction. Thus, a comparison of electrode composite material HSPs can provide insight into the physical interactions between the components and thereby provide a quantitative view of materials dispersion.

Using the solubility and/or dispersivity of the component materials in a range of solvents with known HSPs, materials HSPs can be calculated by Hansen software (Hansen Solubility Parameters in Practice third edition). HSPs (δ_D, δ_P and δ_H) and the radius (R_o) of the sphere of interaction for the materials can be obtained, wherein solvents within R_o can be expected to dissolve/disperse the solute. The parameters, δ_D, δ_P and δ_H, are related to the (atomic) dispersion forces, (molecular) permanent dipole-permanent dipole forces and (molecular) hydrogen bonding, respectively.[42–45] Furthermore, to evaluate whether or not a solvent belongs to a sphere of high

physical affinity, the distance R_a between the solvent and the material is calculated by Eq. 1,

$$(R_a)^2 = 4(\delta_{D1} - \delta_{D2})^2 + (\delta_{P1} - \delta_{P2})^2 + (\delta_{H1} - \delta_{H2})^2 \quad (1)$$

where the subscripts 1 and 2 represent the solute and solvent, respectively. The relative energy difference (RED=R_a/R_o) provides an estimate of whether two materials will be miscible (miscible when RED < 1, partially miscible when RED = 1 and immiscible when RED > 1).[45] In this investigation, nanoparticles were judged to be dispersible when RED was less than 1. The result of solubility tests in a wide range of solvents is summarized in Supporting Information.

As shown in **Figure 4**, RED was calculated for OA-Fe_3O_4 and Super-P carbon additives with respect to PVDF and P3HT. For OA-Fe_3O_4, the RED of PVDF and P3HT is 1.86 and 1.04, respectively; for Super-P, the PVDF value is 0.82 and that of P3HT is 0.85. The calculated OA-Fe_3O_4 RED values support the optical microscopy observations (*vide supra*). The RED value calculated for Super-P with PVDF is unexpected, and suggests that carbon additives should be dispersible in PVDF. Examination of the RED with different solvents, chloroform has a value of 0.63 for Super-P, whereas NMP exhibits an RED of 1.00 (note: OA-Fe_3O_4: chloroform 1.04, NMP 1.86). Thus, solvent-electrode component interactions during electrode processing also play an important role in determining the material dispersion state. In other words, the carbon aggregates seen in the PVDF system (**Figure 2**) might be ascribed to poor/inferior physical affinity between the Super-P carbon additive and NMP solvent inducing poor dispersion, even though carbon and PVDF have good physical affinity. On a cautionary note, this investigation is limited to estimating the physical interaction between just two materials; the gross physical interactions present among active nanoparticles, carbon additives, polymeric binder, and even solvent could significantly impact final processed morphology.

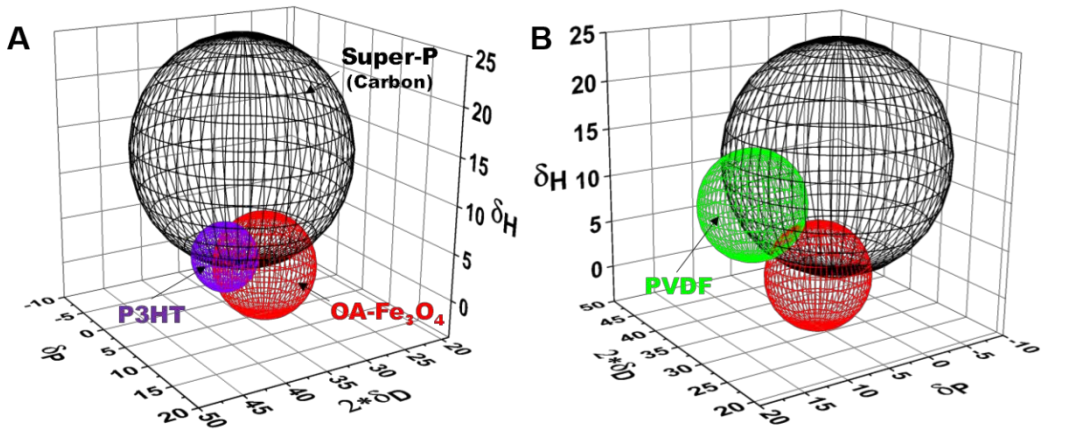

Material	δ_H (MPa$^{1/2}$)	δ_P (MPa$^{1/2}$)	δ_D (MPa$^{1/2}$)	R_o (MPa$^{1/2}$)	Data fit
OA-Fe_3O_4	1.25	4.57	16.12	5.7	0.992
Super-P	12.87	2.42	17.63	11.4	1.000
PVDF	9.14	11.05	17.57	5.7	1.000
P3HT	3.49	3.39	18.8	3	1.000

Material	$\%V_{int}$ [1)]	
	P3HT	PVDF
OA-Fe_3O_4	34.9	0.69
Super-P	85.0	66.4

[1)] $\%V_{int} = V_{int} / V_{polymer}$ x 100

Figure 4. Hansen solubility parameter (HSP) spheres of interaction for (A) OA-Fe_3O_4/carbon/P3HT and (B) OA-Fe_3O_4/carbon/PVDF. Tables show HSPs of the composite battery electrode components and superimposed volume portions ($\%V_{int}$) for each polymer volume ($V_{polymer}$).

The Hansen spheres in **Figure 4** show the regional relationship of interactions for OA-Fe_3O_4/carbon/P3HT and OA-Fe_3O_4/carbon/PVDF. Generally, when regions of affinity/solubility for different materials are superimposed, the components are expected to experience very high physical attraction.[43] Together with the RED value, in order to confirm the extent of overlap between two spheres of interaction, the sphere intersection volume (V_{int}) was calculated and the superimposed volume portion ($\%V_{int}$) for each polymer volume ($V_{polymer}$) was obtained by V_{int} / $V_{polymer}$ as shown in the table in **Figure 4**.[46] The results of this analysis strongly suggest that OA-Fe_3O_4 and Super-P carbon additives have more favorable physical affinity with P3HT vs. PVDF. The insights gained from evaluation of the sphere intersection volume appear more suitable than RED to predict the dispersivity of battery electrode materials.

The propensity of OA-Fe_3O_4 to disperse uniformly within P3HT might also result from surface interactions. The contact angle of an OA droplet on the surface of the polymer film provides

one measure of the physical interactions between the two materials. Typically, the contact angle decreases when the extent of physical attraction increases.[47] As shown in **Figure 5A,** OA exhibits a lower contact angle on PVDF than P3HT, which implies good physical affinity with PVDF. These results concur with estimates of RED for OA with P3HT (4.69) and PVDF (2.02) (see table in **Figure 5;** a smaller RED suggests better miscibility); however, they contradict experimental OA-Fe_3O_4-based composite observations.

Considering OA-Fe_3O_4 nanoparticle structure, only the hydrophobic OA tail is relevant, because the capping agent's -COOH groups would be chemically bound to the Fe_3O_4surface. Accordingly, the measured contact angle may not be a fully reflective measure to judge the physical affinity between the capped nanoparticles and polymer binders. Alternatively, the HSP approach may be predictive. As illustrated in **Figure 5B**, OA exhibits two HSP spheres[48]; one associated with the unsaturated hydrocarbon tail (OA-Hydrophobic), the second for the carboxylic acid moiety (OA-COOH). For OA-Hydrophobic, the RED and intersection volume portion (%V_{int}) for PVDF and P3HT are 1.64/4.2% and 0.66/87.5%, respectively. In the case of OA-Hydrophobic and P3HT, the two spheres are almost superimposed indicating the close nature of the HSP regions. Consequently, their physical affinities towards other materials are expected to be comparable.[43] Thus, in order to effectively evaluate the physical affinities/interactions between materials comprising a composite, all aspects of molecular structure must be considered. HSP analysis provides an effective strategy to evaluate interactions between components which can then suggest approaches to modify relevant surfaces. Taken together, the approach might prove powerful to aid identification of strategies to improve materials dispersity in battery electrodes.

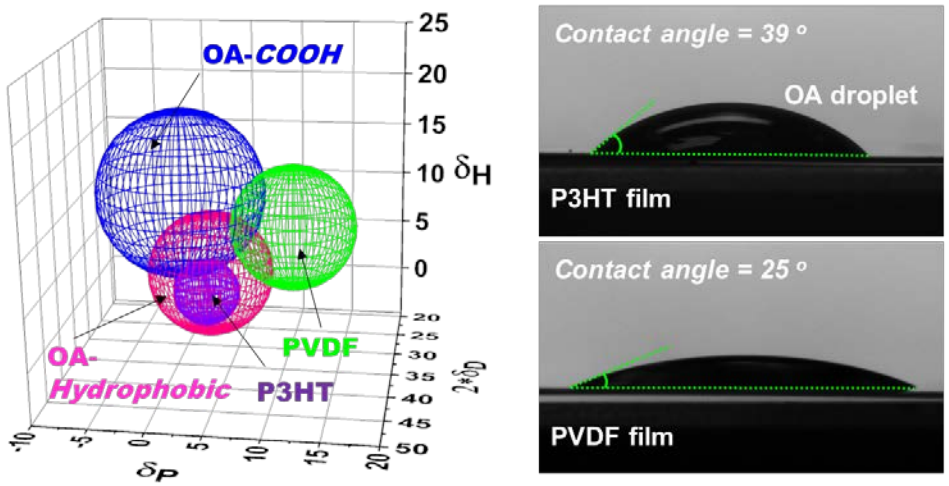

Material	δ_H (MPa$^{1/2}$)	δ_P (MPa$^{1/2}$)	δ_D (MPa$^{1/2}$)	R_o (MPa$^{1/2}$)	R_a (MPa$^{1/2}$)		RED	
					P3HT	PVDF	P3HT	PVDF
OA-*Hydrophobic* [1)]	4	3.1	16.9	5.78	3.84	9.56	0.66	1.64
OA-*COOH* [1)]	11.4	0.3	16.5	7.88	9.66	11.19	1.23	1.42
OA [2)]	14.3	3.1	14.3	-	14.07	11.52	4.69	2.02

[1)] Calculated by Hansen software[48]
[2)] Value form Hansen's 1971 parameters listed in Handbook of Solubility Parameters[60]

Figure 5. Surface physical affinities between oleic acid (OA) and polymer (P3HT & PVDF): (A) contact angle measurement (OA droplet on polymer film) and (B) HSP spheres of interaction. Table represents the values of HSP, R_a and RED. The RED of unsaturated hydrocarbon part of OA (OA-Hydrophobic) with P3HT is less than 1, predicting they are miscible.

Electrical Properties. It has been demonstrated that composite materials morphology influences electrode performance.[49–51] In particular, the dispersion of active materials and carbon additives can affect the current distribution over the composite electrode during electrochemical testing. The current distribution directly impacts battery performance. Thus, it would be anticipated that the material dispersion state would also be connected to battery electrode electrical properties such as electronic conductivity. The development of reliable and robust experimental techniques that can directly measure electronic conductivity without interference from the metal foil substrate, however, is a challenge. Existing techniques such as electrochemical impedance spectroscopy (EIS) and point probe measurement have some limitations. For instance, for EIS, it is difficult to separate electronic

and ionic resistances in the presence of electrolyte, while for the point probe method, it is difficult to maintain sufficient contact with porous, composite films without damage as well as to keep the applied pressure of the probe constant.[52,53] Hence here, a newly designed electrode device for measuring electronic conductivity of composite battery electrode materials is introduced; the device is similar to a Field-Effect Transistor (FET).[54,55]

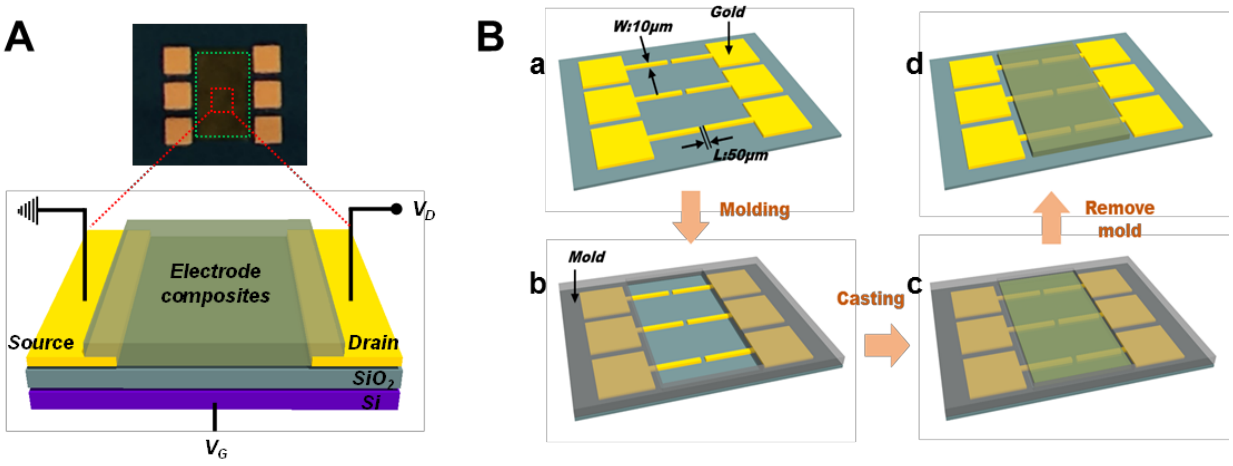

Figure 6. (A) Schematic structure and photo-image of bottom contact electrode device. (B) Schematic diagram of mold casting process showing fabrication of the electrode devices for measuring the electronic conductivity. The respective composite slurries were mold-casted onto the device substrates (channel width = 10 μm and length = 50 μm). The thickness of composite films was approx. 4~10μm.

For the electrical measurements, we adopted the newly designed configuration (channel width = 10 μm and length = 50 μm) (**Figure 6A**) with two bottom contacts, allowing for measurements of contact resistance. Composite electrode electronic conductivity is measured simultaneously at three different points, thereby providing insight as to the uniformity of the distribution of the electronically conductive channels. Two voltage probes between the source and drain electrodes monitor the potential along the conductive channel, consequently inducing mobile charge carriers.[54] The resulting electronic conductivity was calculated by Eq.2

$$\sigma = \frac{L}{W \times t}\frac{I_D}{V_D} \qquad (2)$$

where W (10 μm), L (50 μm) and t are the channel width, length and film thickness, respectively. V_D is the drain voltage, and I_D is the drain current.

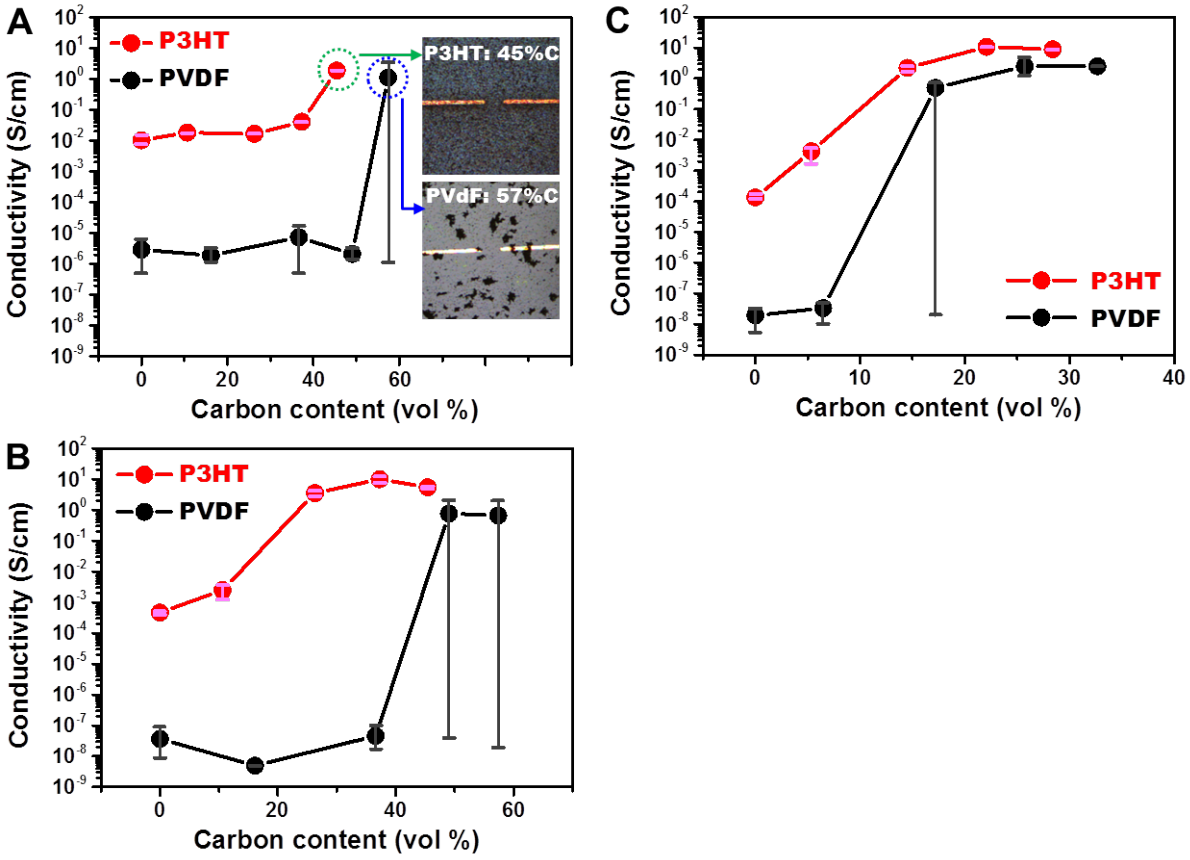

Figure 7. Electronic conductivities of (A) carbon/polymer composites (spin-coating method): inset figures showing the OM images of 45 vol. % of carbon/P3HT and 57% vol. % of carbon/PVDF which are considered the percolation threshold concentration in spin-coated electrodes, (B) carbon/polymer composites (mold-casting method) and (C) OA-Fe_3O_4/carbon/polymer composites (mold-casting method) with constant amount of OA-Fe_3O_4 and polymer. The graph has the sphere symbols expressing the average conductivity, together with the upper bar for the largest value and the lower bar for the smallest value.

The composite film layers were prepared by spin coating and mold casting. The electronic conductivity associated with spin coating, as shown in **Figure 7A**, correlates with the OM observation results in **Figure 2B**; P3HT with uniformly dispersed carbon additives exhibits electronic conductivities having no deviation, whereas carbon obviously aggregates in the PVDF counterpart and large deviations are observed, notably at about 57 vol. % carbon. The results

strongly suggest that the improved electrical properties derive from the more uniformly dispersed P3HT system. The electronic conductivity of devices fabricated by the two methods, however, differs (**Figure 7A and 7B**), particularly for the percolation threshold concentration. Although the electrode prepared by spin coating has the advantage of facilitating differentiation of the material dispersion state via readily accessible techniques such as optical microscopy and accurately representing the enhanced electrical properties associated with the respective morphologies, the percolation networks generated between two channels (10 μm) vary from the more representative dense electrodes. Most likely, this results from the spread-out morphology of spin-coated electrodes (inset images in **Figure 7A**). Thus, mold casting was used as the electrode fabrication method, whereby a rectangular mold was used to make the dense electrode, as depicted in **Figure 6B**. Specifically, after a mold is placed on the patterned electrode device, the as-prepared slurry was cast into the mold and then solvent was evaporated. The photo-image in **Figure 6A** represents the electrode device coated by mold casting (green rectangle). For the carbon/polymer composite electrodes (**Figure 7B**), the P3HT system exhibits a conductive percolation threshold at about 26 vol. % carbon, while that for the PVDF counterpart is about 45 vol. %. In addition, the P3HT system conductivity shows almost no deviation, whereas PVDF requires over 48 vol. % carbon and the composite has many fewer conductive regions despite exhibiting percolation behavior. For the OA-Fe_3O_4/carbon/polymer composites **(Figure 7C**), even though both systems have similar percolation thresholds, the electronic conductivity of the PVDF-17 vol. % carbon electrode exhibits the same small value, ~10^{-8} S/cm, as that prepared with under 7 vol. % carbon. These results provide further evidence that the dispersion state of the electrode materials has a significant effect on properties such as electronic conductivity; more well-dispersed battery materials provide for enhanced electrical characteristics. Accordingly, it might be expected that P3HT-based electrodes will experience more homogeneous current distribution over the uniformly dispersed components of a composite electrode vs PVDF-based counterparts with uneven current distribution.

Electrochemical Evaluation. Four combinations of electrode components were tested in an experimental two electrode coin cell configuration versus lithium metal: 1) P3HT with uncapped Fe_3O_4, 2) PVDF with uncapped Fe_3O_4, 3) P3HT with OA-Fe_3O_4 and 4) PVDF with OA-Fe_3O_4. Each electrode was lithiated from open-circuit potential to 0.3 V then delithiated to 3.0 V vs. Li/Li^+. The lithiation and delithiation voltage profiles for each electrode type are shown in **Figure 8**. During lithiation, electrodes with uncapped Fe_3O_4 produced 1,334 mAh/g with P3HT binder and a similar 1,300 mAh/g with PVDF. Samples with uncapped Fe_3O_4 with either binder operated at similar operating voltages with plateaus of 1.63, 1.18 and 0.90 V. The sample with uncapped Fe_3O_4 and PVDF demonstrated 830 mAh/g on delithiation while the capacity for the P3HT sample was 739 mAh/g. Cells with OA-Fe_3O_4 and PVDF binder delivered 600 mAh/g and those with P3HT binder delivered 125 mAh/g. Additionally, the cell with P3HT and oleic acid-capped magnetite showed a lower lithiation voltage (~0.5 V).

Electrodes fabricated with oleic acid-capped Fe_3O_4 showed better particle dispersion and worse electrochemical performance than cells with uncapped Fe_3O_4. It was hypothesized that evenly distributed particles would expose more surface area of the active material to the electrolyte and shorten Li^+ ion diffusion pathways. There can be slow diffusion paths to the center of large particle agglomerates which limit gravimetric capacity as some active material is isolated in the agglomerate center and inaccessible to Li^+ ions.[5,12,56] Both P3HT and PVDF displayed significant agglomeration with uncapped Fe_3O_4 but they outperformed electrodes with OA-capped Fe_3O_4. These results suggest that oleic acid has an additional, significant impact on electrochemical performance beyond particle dispersivity. The use of oleic acid decreased capacity which is likely due to poor electron transport or Li^+ ion diffusion through the layer of oleic acid surrounding the active particles. It is possible that oleic acid acted as an insulating shell around the active material. Poor electron or ion transport through the electrode can be visualized as an increase in electrode electrical resistance. AC impedance was measured to investigate differences in resistances of the assembled coin cells.

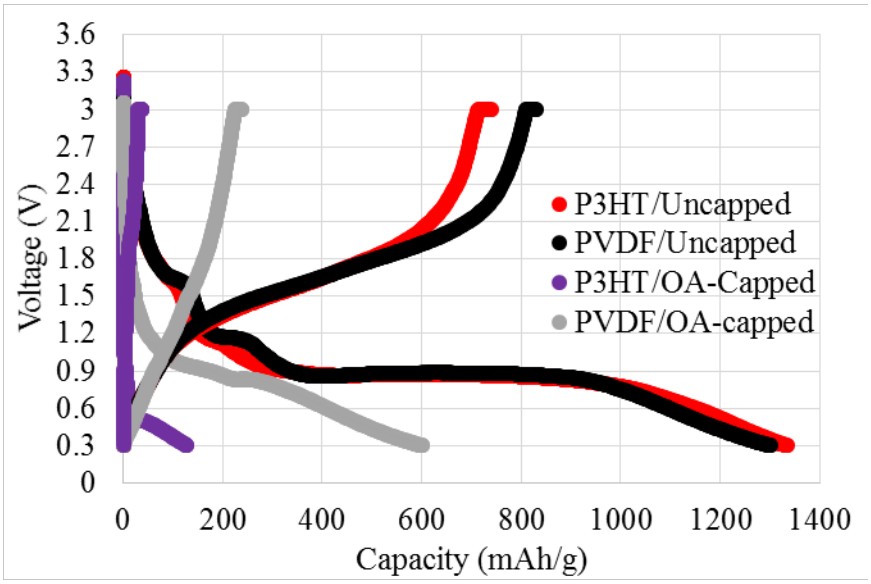

Figure 8. Voltage profiles for Li/Fe_3O_4 electrochemical cells.

AC impedance spectroscopy of the coin cells was performed prior to operation, **Figure 9**. AC impedance spectroscopy can be used to measure a battery's ionic and electronic conductivities. P3HT/uncapped Fe_3O_4, PVDF/uncapped Fe_3O_4 and PVDF/OA-Fe_3O_4 samples displayed AC responses showing a depressed semicircle at higher frequencies followed by a long linear tail at lower frequencies. This type of Nyquist plot can be fit with the equivalent circuit shown in **Figure 9D**. In this model, Rs is the ohmic series resistance, Rct is related to the charge-transfer resistance of the cathode and the Warburg element is related to ionic diffusion. The P3HT and OA-Fe_3O_4 showed significantly larger impedance. Absolute impedance Z' is plotted against frequency in **Figure 9C**. All samples responded similarly to higher frequencies, but differed greatly at low frequencies. At 0.01 Hz the absolute impedance of P3HT/OA-Fe_3O_4 is more than 100 times greater than both samples with uncapped magnetite while the sample with PVDF/OA-Fe_3O_4 had an absolute impedance more than 15 times the impedance of the uncapped samples. Results from the equivalent circuit fits are displayed in **Figure 9E**. The Warburg coefficient was taken as the slope of the relationship between absolute impedance (Z') and the inverse square root of angular frequency ($\omega^{-1/2}$) at low frequencies.

Each cell showed similar Rs values as expected. Comparing the two samples with uncapped Fe_3O_4 show that the electrode with P3HT exhibited nearly double the charge transfer resistance and a larger Warburg coefficient compared to PVDF. The electrodes with PVDF indicate that the presence of oleic acid increases charge transfer resistance and significantly increases the Warburg coefficient. The Warburg coefficient in the P3HT/OA-Fe_3O_4 sample is large which indicates that ion diffusion is limited in this electrode.

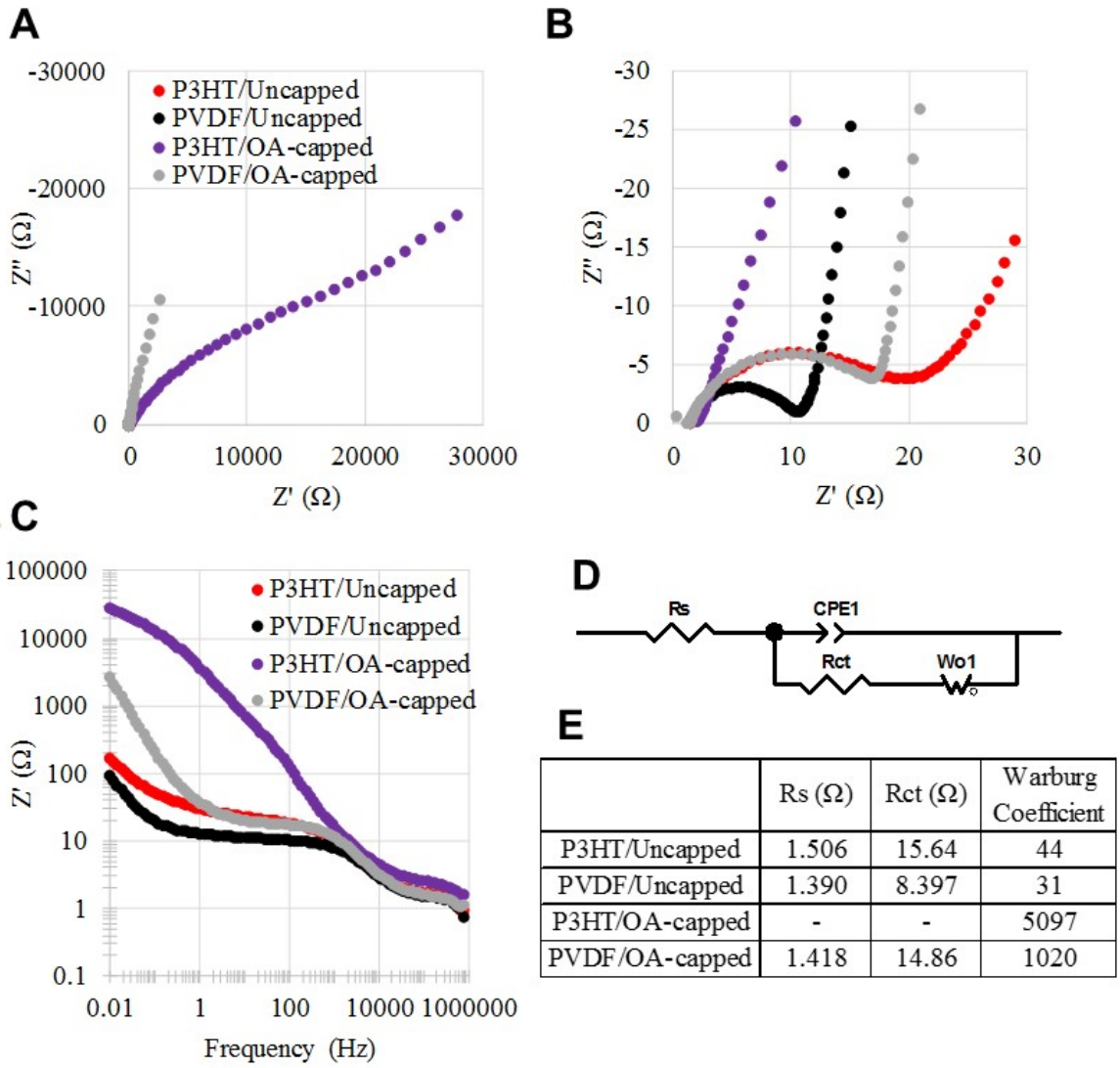

	Rs (Ω)	Rct (Ω)	Warburg Coefficient
P3HT/Uncapped	1.506	15.64	44
PVDF/Uncapped	1.390	8.397	31
P3HT/OA-capped	-	-	5097
PVDF/OA-capped	1.418	14.86	1020

Figure 9. Electrochemical Impedance Spectroscopy (EIS) results for Li/Fe_3O_4 electrochemical cells before cycling. (A) Nyquist plot of EIS results, (B) Nyquist plot of EIS results with smaller axes values, (C) Bode plot of EIS results, (D) equivalent circuit used to fit EIS data, and (E) results from

fitting EIS with equivalent circuit.

The delivered capacities of uncapped magnetite (Fe_3O_4) electrodes prepared with P3HT or PVDF binders were similar. These results are consistent with the impedance results for the two systems, which are also similar. The capacities of the electrodes containing OA-Fe_3O_4 were significantly lower than those using pristine Fe_3O_4. As oleic acid coats the Fe_3O_4 particles it interferes with the electrochemical activity of magnetite in the electrode coating. Oleic acid as a capping agent improves particle dispersion, but capping agents can also negatively influence electrochemical results by restricting ion and possibly electron transport. The cells containing P3HT and OA-capped Fe_3O_4 displayed the poorest electrochemical performance of the group. This cathode combination produced the lowest capacity and lowest operating voltage.

Previously, oleic acid capped Fe_3O_4 nanoparticles dispersed on a glassy carbon electrode surface were evaluated electrochemically.[57] Cyclic voltammetry of the coated electrodes was performed in acidic aqueous media and demonstrated that while the Fe_3O_4 was electrochemically active, the delivered current was lower than anticipated based on estimates from the film thickness. It was noted that a significant fraction of magnetite was not electrochemically accessible; the cause was broadly assigned to nanoparticle aggregation, limited transport through the Nafion film that was used or the presence of oleic acid.

The electrochemical results here provide several findings. In comparison to the performance of cells prepared with PVDF and uncapped magnetite, the P3HT counterparts exhibit somewhat higher charge transfer resistance. The similar lithiation and lower delithiation capacity of the P3HT cells are consistent with the impedance results. The combined EIS and constant current cycling results indicate that the electrochemical behavior of uncapped Fe_3O_4 is superior to that of OA- Fe_3O_4. The presence of the oleic acid capping agent increases the charge transfer resistance in both polymeric binder environments. The impact on electrochemistry of oleic acid is much more

significant when P3HT serves as the binder vs. PVDF. As evidenced by the increased Warburg coefficient, oleic acid appears to severely limit ion transport in both systems. The effect is more significant in the P3HT environment.

The results presented in this investigation show that capping agents can effectively stabilize and promote improved nanoparticle dispersion; however that dispersivity is highly system dependent. With respect to composite battery electrodes, the active material, conductor and binder all play a role in performance. Through studies using capped and uncapped Fe_3O_4, and two alternative binder polymers, it was demonstrated that materials dispersivity cannot be used in isolation to predict electrochemical performance. For instance, separate previous studies strongly suggested that oleic acid coated active materials would positively impact electrode performance and/or conjugated polymer electronic conductivity. Here, it was shown that capping agents can be detrimental to electrochemical performance. Electronic conductivity, electron transfer as well as ion transport impact electrochemical behavior and must all be considered in the design of active material environments. This report provides insight for future studies pertaining to dispersion of active nanomaterials, surface modifications, and compatibility with polymeric binders.

CONCLUSION

Surface modification of nanoparticles used for composite battery electrode applications has been shown to be an effective strategy to achieve remarkably enhanced materials dispersivity. Effective approaches include the introduction of surfactant-like functionalities onto electroactive materials via organic capping agents and wrapping of carbon additives with conjugated polymers. In addition, deliberate consideration of particle surface physical affinities/interactions aided by Hansen solubility parameter analysis helps to illuminate component surface characteristics, and thereby facilitate the design of compatible architectures. A simple spin coating process which affords a thin-film can simplify characterization of the component materials dispersion state via optical, atomic force and

scanning electron microscopies.

It is anticipated that the use of physical affinity relationships will enable the design and fabrication of more uniformly dispersed composites for battery electrode applications; improved dispersion characteristics are expected to enhance both electrical and electrochemical properties. Notably, electronic conductivity, electron transfer as well as ion transport impact electrochemical behavior and must all be considered in the design of active material environments. The approaches described herein are expected to provide fundamental insights into the mechanisms and impact of uniform dispersion in battery electrode applications, especially for the effective incorporation and utilization of electroactive nanomaterials components.

EXPERIMENTAL SECTION

Materials. Fe_3O_4, magnetite, was synthesized using a previously reported coprecipitation approach, using aqueous solution of iron(III) chloride hexahydrate, iron(II) chloride hexahydrate, trimethylamine.[58,59] For preparation of Fe_3O_4 nanoparticles capped with oleic acid (OA-Fe_3O_4),[22] 4ml of oleic acid was added to 0.3g Fe_3O_4 nanoparticles prepared above and followed by stirring the solution for 24 h. The OA-Fe_3O_4 powder was extracted after sonication by centrifuge separation with 15 mL acetone with speed of 9000 rpm for 2 mins for 3 times. P3HT was purchased from Rieke Metals Inc. The molecular weight of P3HT (M_n of 19.6 kDa and M_w of 43.7 kDa) used for the study was measured by gel permeation chromatography (GPC). The head to tail regioregularity (RR) was estimated to be approximately 96% (Bruker DSX 300 ^{1}H NMR in deuterated chloroform solution at 293K).

Composite Electrode Fabrication. The slurries for the P3HT-based electrode were prepared by mixing of OA-Fe_3O_4, Super-P carbon additive, and P3HT in a solvent of chloroform, and in case of PVDF-based electrode, NMP solvent was used with the same composition of P3HT-based electrode.

The only carbon content was changed with OA-Fe_3O_4 and Super-P kept constant. Super-P/polymer composite followed the previous procedure, except for OA-Fe_3O_4. The solid content was 3.4 wt % for spin coating and mold casting, and 27 wt % for blade coating. The electrodes for the measurements of OM, AFM, FE-SEM, and electronic conductivity were prepared by spin-coating (WS-6500MZ-23NPP, Laurell) the slurries onto substrates at the spin rate of 1500 rpm for 60 sec in air. The electrodes for FE-SEM measurement and electrochemical evaluation were produced by blade coating (doctor blade, MTI corp). Mold casting was conducted using a rectangular mold being put onto the substrate for measuring the electronic conductivity. These prepared electrodes were pre-evaporated at 70 ^oC for 1hr and completely evaporated at 130 ^oC for 12 hr in a vacuum oven.

Morphology Characterization. The optical Microscopy (OM) measurements were conducted on the composite films spin-coated on the glass substrate using Olympus MX61 Microscope. The Atomic Force Microscopy (AFM) images were obtained with an ICON dimension scanning probe microscope (Bruker) using tapping mode with a silicon tip (RTESP, Bruker). The Field Emission-Scanning Electron Microscopy (FE-SEM) images were observed on the top view of the electrodes using Zeiss Ultra-60 FE-SEM.

Hansen Solubility Parameter (HSP) Characterization. Polymer (10mg) such as P3HT and PVDF, Super-P carbon particles (0.5mg) and OA-Fe_3O_4 nanoparticles (10mg) were placed into a vial with 3 mL of a test solvent, respectively (see Supporting Information on the result of solubility tests).[43–45] The vial was heated at 70 ^oC for 3 hr and sonicated for 60 min and after then the vials were permitted to stand and observed for 6 hr in ambient temperature. The dispersion stability was examined by these solutions via visual observation. In case of polymer, solvents would be considered as poor if they were unable to dissolve the polymer after dissolving process and good if they were able to dissolve it.[45] For the particles including OA-Fe_3O_4 and Super-P, solvents would be classified as poor when they were completely deposited on the vial bottom after 60 min sonication, and solvents would

be good when sedimentation on the vial bottom required more than 6 hr after the sonication step.[43] Based on the visual examination, Hansen solubility parameters (δ_D, δ_P and δ_H) and the radius value (R_o) of the sphere of interaction were calculated and fitted by HSPiP software (Hansen Solubility Parameters in Practice third edition).

Electronic Conductivity Measurement. The electrode devices with two bottom contacts (channel width = 10 μm and length = 50 μm) were used for electrical characterization, where composite film was deposited via spin coating or mold casting on a silicon wafer with a 300 nm thick SiO_2. The characterization process is as follows[55]: Au was used for the source and drain contacts which were fabricated using a standard photolithography based on lift-off process, followed by Denton Explorer E-beam evaporation of 3 nm thick Cr as the adhesive layer and sequentially Au contact with 50 nm thickness. Before coating, all devices were exposed in a UV-ozone cleaner (Novascan PSD-UV) for 15 min to completely remove of any organic containments. The prepared composite electrodes described in previous section were tested in nitrogen ambient using a semiconductor parameter analyzer (Agilent 4155C).

Electrochemical Characterization. Stainless steel coin cells were constructed with Li anodes, polymeric separators and cathodes comprised of composite coatings (15% Super P, 14% polymer binder and 71% Fe_3O_4) on copper foil. Electrodes used in coin cells were created by coating a slurry mixture onto copper foil with a doctor blade. After the solvent evaporated, 0.5 inch diameter electrodes were punched from the coating and pressed. Electrolyte consisted of 1 M $LiPF_6$ salt in a mixture of ethylene carbonate:dimethyl carbonate in a volume ratio of 30:70. Coin cells were tested by lithiating Fe_3O_4 to 0.3 V and then delithiating to 3.0 V at rates of 20 mA per gram of Fe_3O_4 in the electrode coating at 30^{o}C. After reaching 3.0 V cells were held at constant voltage for 1 hr. AC Impedance Spectroscopy was measured using a Bio-Logic potentiostat over a frequency range of 1.0 mHz and 1 MHz. Three coin cells were built with each electrode type. All cells showed similar

trends in capacity and impedance with respect to electrode type. One representative cell of each electrode type is reported here.

ASSOCIATED CONTENT

Supporting Information

Solubility tests for Hansen solubility parameter of OA-Fe_3O_4, Super-P, P3HT, and PVDF and AFM images of OA- Fe_3O_4/carbon/P3HT composites.

AUTHOR INFORMATION

Corresponding Authors

*E-mail: esther.takeuchi@stonybrook.edu.

*E-mail: ereichmanis@chbe.gatech.edu.

ACKNOWLEDGMENTS

This work was performed as part of the Center for Mesoscale Transport Properties, an Energy Frontier Research Center supported by the U.S. Department of Energy, Office of Science, Basic Energy Sciences, under award #DE-SC0012673. MMH acknowledges that this material is based upon work supported by the National Science Foundation Graduate Research Fellowship Program under Grant No. 1109408.

REFERENCES

(1) Armand, M.; Tarascon, J. M. Building Better Batteries. *Nature* **2008**, *451*, 652–657.

(2) Armand, M.; Tarascon, J. M. Issues and Challenges Facing Rechargeable Lithium Batteries. *Nature* **2001**, *414*, 359–367.

(3) Arico, A. S.; Bruce, P.; Scrosati, B.; Tarascon, J. M.; Schalkwijk, W. V. Nanostructured Materials for Advanced Energy Conversion and Storage Devices. *Nature Materials* **2005**, *4*, 366–377.

(4) Chen, H.; Wang, C.; Dong, W.; Lu, W.; Du, Z.; Chen, L. Monodispersed Sulfur Nanoparticles for Lithium−Sulfur Batteries with Theoretical Performance. *Nano Lett.* **2015**, *15*, 798–802.

(5) Bock, D. C.; Kirshenbaum, K. C.; Wang, J.; Zhang, W.; Wang, F.; Wang, J.; Marschilok, A. C.; Takeuchi, K. J.; Takeuchi, E. S. 2D Cross Sectional Analysis and Associated Electrochemistry of Composite Electrodes Containing Dispersed Agglomerates of Nanocrystalline Magnetite, Fe3O4. *ACS Appl. Mater. Interfaces* **2015**, *7*, 13457–13466.

(6) Kang, B.; Ceder, G. Battery Materials for Ultrafast Charging and Discharging. *Nature* **2009**, *458*, 190–193.

(7) Zhang, W. M.; Wu, X. L.; Hu, J. S.; Guo, Y. G.; Wan, L. J. Carbon Coated Fe3O4 Nanospindles as a Superior Anode Material for Lithium-Ion Batteries. *Adv. Funct. Mater.* **2008**, *18*, 3941–3946.

(8) de Guzman, R. C.; Yang, J.; Cheng, M. C. M.; Salley, S. O.; Ng, K. Y. S. A Silicon Nanoparticle/Reduced Graphene Oxide Composite Anode with Excellent Nanoparticle Dispersion to Improve Lithium ion Battery Performance. *J. Mater. Sci.* **2013**, *48*, 4823–4833.

(9) Tao, T.; Glushenkov, A. M.; Zhang, C.; Zhang, H.; Zhou, D.; Guo, Z.; Liu, H. K.; Chen, Q.; Hub. H.; Chena, Y. MoO_3 Nanoparticles Dispersed Uniformly in Carbon Matrix: a High Capacity Composite Anode for Li-ion Batteries. *J. Mater. Chem.* **2011**, *21*, 9350–9355.

(10) Lee, J. K.; Smith, K. B.; Hayner, C. M.; Kung, H. H. Silicon Nanoparticles–Graphene Paper Composites for Li ion Battery Anodes. *Chem. Commun.* **2010**, *46*, 2025–2027.

(11) Kim, J. S.; Nguyen, C. C.; Kim, H. J.; Song, S. W. Siloxane-capped Amorphous Nano-SiOx/Graphite with Improved Dispersion Ability and Battery Anode Performance. *RSC Adv.* **2014**, *4*, 12878–12881.

(12) Knehr, K. W.; Brady, N. W.; Cama, C. A.; Bock, D. C.; Lin, Z.; Lininger, C. N.; Marschilok, A. C.; Takeuchi, K. J.; Takeuchi, E. S.; West, A. C. Modeling the Mesoscale Transport of Lithium-Magnetite Electrodes Using Insight from Discharge and Voltage Recovery Experiments. *J. Electrochem. Soc.* **2015**, *162*, A2817−A2826.

(13) Bhattacharya, S.; Srivastava, A.; Pal, A. Modulation of Viscoelastic Properties of Physical Gels by Nanoparticle Doping: Influence of the Nanoparticle Capping Agent. *Angew. Chem.* **2006**, *118*, 3000–3003.

(14) Corbierre, M. K.; Cameron, N. S.; Sutton, M.; Laaziri, K.; Lennox, R. B. Gold Nanoparticle/Polymer Nanocomposites: Dispersion of Nanoparticles as a Function of Capping Agent Molecular Weight and Grafting Density. *Langmuir* **2005,** *21*, 6063-6072.

(15) Saunders, B. R.; Turner, M. L. Nanoparticle–Polymer Photovoltaic Cells. *Adv. Colloid Interfac.* **2008**, *138*, 1–23.

(16) Tang, J.; Kemp, K. W.; Hoogland, S.; Jeong, K. S.; Liu, H.; Levina, L.; Furukawa, M.; Wang, X.; Debnath, R.; Cha, D.; Chou, K. W.; Fischer, A.; Amassian, A.; Asbury, J. B.; Sargent, E. H. Colloidal-Quantum-Dot Photovoltaics using Atomic-Ligand Passivation. *Nature Materials* **2011**, *10*, 765–771.

(17) Singh, A. K.; Viswanath, V.; Janu, V. C. Synthesis, Effect of Capping Agents, Structural, Optical and Photoluminescence Properties of ZnO Nanoparticles. *J. Luminescence* **2009**, *129*, 874–878.

(18) Green, M.; Harwood, H.; Barrowman, C.; Rahman, P.; Eggeman, A.; Festry, F.; Dobsonb, P.; Ng, T. A Facile Route to CdTe Nanoparticles and their Use in Bio-Labelling. *J. Mater. Chem.* **2007**, *17*, 1989–1994.

(19) Park, H. Y.; Schadt, M. J.; Wang, L.; Lim, I. S.; Njoki, P. P.; Kim, S. H.; Jang, M. Y.; Luo, J.; Zhong, C. J. Fabrication of Magnetic Core@Shell Fe Oxide@Au Nanoparticles for Interfacial Bioactivity and Bio-separation. *Langmuir* **2007**, *23*, 9050-9056.

(20) Cozzoli, P. D.; Kornowski, A.; Weller. H. Low-Temperature Synthesis of Soluble and Processable Organic-Capped Anatase TiO2 Nanorods. *J. AM. CHEM. SOC.* **2003**, *125*, 14539-14548.

(21) Jadhava, N. V.; Prasadb, A. I.; Kumara, A.; Mishrab, R.; Dharad, S.; Babuc, K. R.; Prajapatc, C. L.; Misrad, N. L.; Ningthoujamb, R. S.; Pandeya, B. N.; Vatsab, R. K. Synthesis of Oleic Acid Functionalized Fe3O4 Magnetic Nanoparticles and Studying Their Interaction with Tumor Cells for Potential Hyperthermia Applications. *Colloids and Surfaces B* **2013**, *108*, 158–168.

(22) Ghosh, R.; Pradhan, L; Devi, L. P.; Meena, S. S.; Tewari, R.; Kumar, A; Sharma, S.; Gajbhiye, N. S.; Vatsa, R. K.; Pandey, B. N.; Ningthoujam, R. S. Induction Heating Studies of Fe3O4 Magnetic Nanoparticles Capped with Oleic Acid and Polyethylene Glycol for Hyperthermia *J. Mater. Chem.* **2011**, *21*, 13388–13398.

(23) Parveen, S.; Rana, S.; Fangueiro, R. A Review on Nanomaterial Dispersion, Microstructure, and Mechanical Properties of Carbon Nanotube and Nanofiber Reinforced Cementitious Composites. *J. Nanomaterails* **2013**, 1–19.

(24) Samanta, S. K.; Fritsch, M.; Scherf, U.; Gomulya, W.; Bisri, S. Z.; Loi, M. A. Conjugated Polymer-Assisted Dispersion of Single-Wall Carbon Nanotubes: The Power of Polymer Wrapping. *Acc. Chem. Res*. **2014**, *47*, 2446−2456.

(25) Islam, M. F.; Rojas, E.; Bergey, D. M.; Johnson, A. T.; Yodh, A. G. High Weight Fraction Surfactant Solubilization of Single-Wall Carbon Nanotubes in Water. Nano Lett. 2003, 3,

269−273.

(26) Liu, J.; Rinzler, A. G.; Dai, H. J.; Hafner, J. H.; Bradley, R. K.; Boul, P. J.; Lu, A.; Iverson, T.; Shelimov, K.; Huffman, C. B.; Rodriguez-Marcias, F. J.; Shon, Y. S.; Lee, T. R.; Colbert, D. T.; Smalley, R. E. Fullerene Pipes. *Science* **1998**, *280*, 1253−1256.

(27) Abdelhamid, M. E.; O'Mullane, A. P.; Snook, G. A. Storing energy in plastics: a review on conducting polymers & their role in electrochemical energy storage. *RSC Adv.* **2015**, *5*, 11611−11626.

(28) Song, C. K.; Eckstein, B. J.; Tam, T. L. D.; Trahey, L.; Marks, T. J. Conjugated Polymer Energy Level Shifts in Lithium-Ion Battery Electrolytes. *ACS Appl. Mater. Interfaces* **2014**, *6*, 19347−19354.

(29) Patel, S. N.; Javier, A. E.; Stone, G. M.; Mullin, S. A.; Balsara, N. P. Simultaneous Conduction of Electronic Charge and Lithium Ions in Block Copolymers. *ACS Nano* **2012**, *6*, 1589−1600.

(30) Patel, S. N.; Javier, A. E.; Balsara, N. P. Electrochemically Oxidized Electronic and Ionic Conducting Nanostructured Block Copolymers for Lithium Battery Electrodes. *ACS Nano* **2013**, *7*, 6056−6068.

(31) Wu, S.-L.; Javier, A. E.; Devaux, D.; Balsara, N. P.; Srinivasan, V. Discharge Characteristics of Lithium Battery Electrodes with a Semiconducting Polymer Studied by Continuum Modeling and Experiment. *J. Electrochem. Soc.* **2014**, *161*, A1836−A1843.

(32) An, H.; Mike, J.; Smith, K. A.; Swank, L.; Lin, Y.-H.; Pesek, S. L.; Verduzco, R.; Lutkenhaus, J. L. Highly Flexible Self-Assembled V2O5 Cathodes Enabled by Conducting Diblock Copolymers. *Scientific Reports* **2015**, *5*, 14166−14176.

(33) Javier, A. E.; Patel, S. N.; Hallinan, D. T.; Srinivasan, V.; Balsara, N. P. Simultaneous Electronic and Ionic Conduction in a Block Copolymer: Application in Lithium Battery Electrodes. *Angewandte Chemie, International Edition* **2011**, *50*, 9848−9851.

(34) Patel, S. N.; Javier, A. E.; Beers, K. M.; Pople, J. A.; Ho, V.; Segalman, R. A.; Balsara, N. P. Morphology and Thermodynamic Properties of a Copolymer with an Electronically Conducting Block: Poly(3-ethylhexylthiophene)-block-poly(ethylene oxide). *Nano Lett.* **2012**, *12*, 4901−4906.

(35) Oschmann, B.; Park, J.; Kim, C.; Char, K.; Sung, Y.-E.; Zentel, R. Copolymerization of Polythiophene and Sulfur To Improve the Electrochemical Performance in Lithium–Sulfur Batteries. *Chem. Mater.* **2015**, *27*, 7011−7017.

(36) Ma, J.; Zhang, X.; Chen, K.; Han, X. Diamond-shaped Fe2O3@C18H34O2 core–shell nanostructures as anodes for lithium ion batteries with high over capacity. *RSC Adv.* **2014**, *4*, 9166−9171.

(37) Guo, S.; Zhang, M.; Zhang, G.; Zheng, L.; Kang, L.; Liu, Z.-H. Synthesis of novel Mn3O4 microsphere and its distinctive capacitance change during electrochemical cycling. *Powder*

Technology **2012**, *228*, 371−376.

(38) Wu, Y.; Li, Y.; Ong, B. S. Printed Silver Ohmic Contacts for High-Mobility Organic Thin-Film Transistors. *J. Am. Chem. Soc.* **2006**, *128*, 4202−4203.

(39) Guerfi, A.; Kaneko, M.; Petitclerc, M.; Mori, M.; Zaghib, K. LiFePO4 water-soluble binder electrode for Li-ion batteries. *J. Power Sources* **2007**, *163*, 1047−1052.

(40) Chou, K.-S.; Huang, K.-C.; Lee, H.-H. Fabrication and sintering effect on the morphologies and conductivity of nano-Ag particle films by the spin coating method. *Nanotechnology* **2005**, *16*, 779−784.

(41) Mihi, A.; Ocana, M.; Miguez, H. Oriented Colloidal-Crystal Thin Films by Spin-Coating Microspheres Dispersed in Volatile Media. *Adv. Mater.* **2006**, *18*, 2244−2249.

(42) Hansen, C. M. *Hansen Solubility Parameters – a User's Handbook*, CRC press: Boca Raton, FL, 2007.

(43) Launay, H.; Hansen, C. M.; Almdal, K. Hansen Solubility Parameters for a Carbon Fiber/Epoxy Composite. *Carbon* **2007**, *45*, 2859–2865.

(44) Bergin, S. D.; Sun, Z.; Rickard, D.; Streich, P. V.; Hamilton, J. P.; Coleman, J. N. Multicomponent Solubility Parameters for Single-Walled Carbon Nanotube–Solvent Mixtures. *ACS Nano* **2009**, *3*, 2340–2350.

(45) Chang, M.; Choi, D.; Fu, B.; Reichmanis, E. Solvent Based Hydrogen Bonding: Impact on Poly(3-hexylthiophene) Nanoscale Morphology and Charge Transport Characteristics. *ACS Nano* **2013**, *7*, 5402–5413.

(46) Weisstein, E. *Sphere–Sphere Intersection*, Eric Weisstein's World of Mathematics, 2009, http://mathworld.wolfram.com/.

(47) Li, X. M.; Reinhoudt, D.; Crego-Calama, M. What Do We Need for a Superhydrophobic Surface? A Review on the Recent Progress in the Preparation of Superhydrophobic Surfaces. *Chem. Soc. Rev.* **2007**, *36*, 1350–1368.

(48) Yamamoto, H. *Hansen Solubility Parameters (HSP) Double Sphere*, 2010, https://pirika.com/.

(49) Zhu, M.; Park, J.; Sastry, A. M. Particle Interaction and Aggregation in Cathode Material of Li-Ion Batteries: A Numerical Study. *J. Electrochem. Soc.* **2011**, *158*, A1155−A1159.

(50) Ligneel, E.; Lestriez, B.; Hudhomme, A.; Guyomard, D. Shaping of Advanced Ceramics: The Case of Composite Electrodes for Lithium Batteries. *J. Eur. Ceram. Soc.* **2009**, *29*, 925−929.

(51) Guy, D.; Lestriez, B.; Bouchet, R.; Guyomarda, D. Critical Role of Polymeric Binders on the Electronic Transport Properties of Composites Electrode. *J. Electrochem. Soc.* **2006**, *153*, A679−A688.

(52) Peterson, S. W.; Wheeler, D. R. Direct Measurements of Effective Electronic Transport in

Porous Li-Ion Electrodes. *J. Electrochem. Soc.* **2014**, *161*, A2175−A2181.

(53) Gomadam, P. M.; Weidner, J. W.; Zawodzinski, T. A.; Saabb, A. P. Theoretical Analysis for Obtaining Physical Properties of Composite Electrodes. *J. Electrochem. Soc.* **2003**, *150*, E371−E376.

(54) Park, B.; Aiyar, A.; Park, M. S.; Srinivasarao, M.; Reichmanis, E. Conducting Channel Formation in Poly(3-hexylthiophene) Field Effect Transistors: Bulk to Interface. *J. Phys. Chem. C* **2011**, *115*, 11719–11726.

(55) Chang, M.; Lee, J.; Kleinhenz, N.; Fu, B.; Reichmanis, E. Photoinduced Anisotropic Supramolecular Assembly and Enhanced Charge Transport of Poly(3-hexylthiophene) Thin Films. *Adv. Funct. Mater.* **2014**, *24*, 4457–4465.

(56) Knehr, K. W.; Brady, N. W.; Lininger, C. N.; Cama, C. A.; Bock, D. C.; Lin, Z.; Marschilok, A. C.; Takeuchi, K. J.; Takeuchi, E. S.; West, A.C. Mesoscale Transport in Magnetite Electrodes for Lithium-Ion Batteries. *ECS Trans.* **2015**, *69*, 7–19.

(57) Murugappan, K.; Silvester, D. S.; Chaudhary, D.; Arrigan, D. W. M. Electrochemical Characterization of an Oleyl-coated Magnetite Nanoparticle-Modified Electrode. *ChemElectroChem* **2014**, *1*, 1211−1218.

(58) Zhu, S.; Marschilok, A. C.; Takeuchi, E. S.; Takeuchi, K. J. Crystallite Size Control and Resulting Electrochemistry of Magnetite, Fe_3O_4. *Electrochem. Solid Stat.* **2009**, *12*, A91–A94.

(59) Zhu, S.; Marschilok, A. C.; Takeuchi, E. S.; Yee, G. T.; Wang, G.; Takeuchi, K. J. Nanocrystalline Magnetite: Synthetic Crystallite Size Control and Resulting Magnetic and Electrochemical Properties. *J. Electrochem. Soc.* **2010**, *157*, A1158−A1163.

(60) Barton, A. F. M. *Handbook of Solubility Parameters and other cohesion parameters*, CRC press, 1983.

Table of Contents